Interacting magnetic defects in a random antiferromagnetic matrix: A spin-glass-like model of exchange bias

M. Gruyters
Institut für Experimentelle und Angewandte Physik, Christian-Albrechts-Universität zu Kiel, 24098 Kiel, Germany
(Received 7 December 2008; revised manuscript received 12 March 2009; published 13 April 2009)

The magnetic behavior of granular CoO layers and granular CoO/ferromagnet bilayers has been investigated by magnetization and hysteresis loop measurements. The net magnetization in the CoO is attributed to magnetic defects due to the particle boundaries and imperfections within the whole particle volume. The CoO particle layers and the CoO/ferromagnet bilayers show characteristic exchange bias effects and a similar magnetization reversal behavior. On the basis of the experimental results, an approach to the problem of exchange bias is suggested. It relies on interacting magnetic defects which are embedded in an antiferromagnetic matrix with a high degree of disorder in the spatial distribution of the magnetic sublattices. The matrix is provided by the antiferromagnetic order within the particles, the spatial disorder by their random anisotropy.

DOI: 10.1103/PhysRevB.79.134415 PACS number(s): 75.50.Lk, 75.30.Gw, 75.70.Cn

I. INTRODUCTION

Exchange bias is a magnetic effect which has been discovered more than 50 years ago[1,2] and which is still at the focus of intensive scientific research.[3,4] In hysteresis loops, it manifests itself as a shift from zero field and an increase in loop width. Usually, at least two material components of different magnetic properties are combined. Ferromagnets, ferrimagnets, antiferromagnets, and spin glasses are examples of these. The most prominent systems in which exchange bias occurs are: particles where the cores couple to the shells,[1,2,5,6] inhomogeneous spin glasses where ferromagnetic (FM) domains couple to antiferromagnetic (AFM) domains,[7] thin films consisting of bilayers[3] where a FM layer couples to an AFM layer, or double superlattices where an artificial FM superlattice couples to an artificial AFM superlattice.[8]

A procedure to establish exchange bias is field cooling the system below the Néel temperature T_N of the antiferromagnet. The resulting hysteresis loop shift H_E is attributed to exchange coupling between the different types of magnetic materials. In the majority of cases, ferro- or ferrimagnets are coupled to antiferromagnets. Direct exchange, superexchange, or indirect exchange may contribute to the underlying microscopic mechanism.[3]

Exchange bias vanishes above a certain temperature which is usually called the blocking temperature T_B.[3] T_B can be appreciably lower than the bulk Néel temperature T_N which is attributed to the spatial dimensions within the antiferromagnet. Below a certain particle or cluster size, the magnetic state becomes unstable against thermal excitations. At temperatures between T_B and T_N, the material is referred to as superparamagnetic. Superparamagnetism strongly depends on magnetic anisotropy and spatial dimensions.[9,10] T_B increases with increasing anisotropy and increasing volume of the particles. The product of both defines a thermal energy barrier of the system. Superparamagnetism is not only important in ensembles of independent particles, but also in inhomogeneous materials with cluster formation and thin films with granular structure. It is one of the characteristic finite-size effects in the magnetism of nanoscaled materials.

A great variety of models exists which aim to describe the properties of exchange bias systems. For AFM/FM bilayers, it has early been suggested that structural disorder especially due to defects plays a decisive role.[11–14] Structural disorder is prevalent at interfaces, either between adjacent layers[4,14,15] or between the core and the shell of particles.[16,17] It strongly influences magnetic properties and appears to be a main source of exchange bias. Structural disorder may lead, e.g., to randomness either in exchange interaction[11] or in anisotropy[18] which, in turn, implies a strong connection to spin-glass-like behavior. Therefore, some of the early[11] and most of the newer models[4,12–14,19–21] of exchange bias have many properties in common with models of spin glasses and other random magnets.[18] Randomness of magnetic properties can also be caused by a granular composition. For example, randomness in particle anisotropy has been considered to be the main source of exchange bias in recent models for AFM particle layers in Ref. 20 and for AFM/FM core-shell particles in Ref. 21.

In this paper, a random anisotropy approach to the problem of exchange bias is suggested. Different from earlier models, it relies on interacting magnetic defects which are embedded in an AFM matrix with a high degree of disorder in the spatial distribution of the magnetic sublattices. Experimental investigations on the magnetic properties of close-packed layers of CoO particles provide the basis for this approach. The CoO particles are arranged in [antiferromagnet/metallic nonmagnet] multilayers and [antiferromagnet/ferromagnet] bilayers.

II. EXPERIMENTAL DETAILS

Hydrogen-passivated Si(111) substrates with a size of $5\times4\times0.35$ mm^3 were prepared *ex situ* by wet chemical treatment. After a final etching in an ammonium fluoride solution, they were carefully introduced into an ultrahigh vacuum apparatus with a base pressure in the low 10^{-10} mbar range following a well-established procedure.[22] In this way, long-range ordered, ideally hydrogen-passivated surfaces were made available for film deposition.

Thin Fe, Co, Ni, and Au films with lateral dimensions of 4×4 mm^2 were grown by molecular-beam epitaxy at a low rate of $1-2$ Å/min after cleanliness and crystalline orienta-

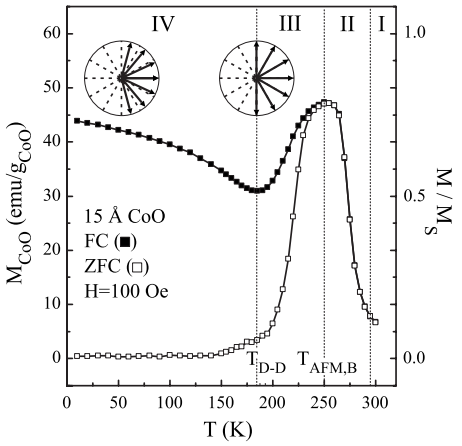

FIG. 1. ZFC and FC magnetizations as a function of increasing temperature T in an external field of $H=100$ Oe for a $[15\ \text{Å CoO}/60\ \text{Å Au}]_{20}$ multilayer sample consisting of 20 layers of close-packed CoO particles. The arrangements of arrows schematically illustrate different orientational configurations of the local magnetization (solid arrows) and the uniaxial anisotropy (dashed lines) of the CoO particles, shown for simplicity in a two-dimensional picture. For further details, see text.

tion of substrate surfaces had been checked by Auger-electron spectroscopy and low energy electron diffraction. The film thickness was monitored by a calibrated water-cooled quartz microbalance. Granular CoO films with constant thickness of 15 or 20 Å were obtained by *in situ* oxidation using a controlled exposure of Co to high-purity oxygen gas.[23,24] In CoO/Au multilayers, Au serves to separate close-packed layers of roundly shaped CoO particles with average lateral diameters of 80–100 Å.[20,23] In order to avoid contamination in air, all samples were capped by 40–70 Å Au.

The magnetic behavior was determined by a Quantum Design superconducting quantum interference device (SQUID) magnetometer. All measurements were performed either after the samples were zero-field cooled (ZFC) or, alternatively, field-cooled (FC) in a positive field $H^{\text{COOL}}=+2.5$ kOe from a temperature of $T=300$ K.

III. MAGNETIC PROPERTIES OF COBALT OXIDE PARTICLE LAYERS

The magnetic behavior of $[15\ \text{Å CoO}/60\ \text{Å Au}]_{20}$ multilayers has been investigated by magnetization and hysteresis loop measurements. In Fig. 1, ZFC and FC magnetizations are shown as a function of increasing temperature in a small external field of $H=100$ Oe. The net magnetization of the CoO originates from the granular structure and the preparation method. Different from ideal AFM bulk materials, not all magnetic Co moments are compensated due to oppositely directed magnetic sublattices. Particle boundaries and defects in the whole particle volume are responsible for the net magnetization M_{CoO}. In this context, it should be noted that the CoO particles with a thickness of 15 Å do neither contain Co cores nor Co clusters of appreciable size which is discussed in detail in Ref. 24.

In the ZFC magnetization curve, the two most prominent features are a zero macroscopic magnetization M_{CoO} for temperatures below 150 K and a peak centered at $T=250$ K. The peak is attributed to superparamagnetic blocking of the AFM order in the CoO particles. This implies that the net magnetization is strongly linked to the spin configuration established by the AFM order. The width and the shape of the peak reflects the particle size distribution.[9] The latter is thus relatively narrow. The onset of instabilities of the AFM order against thermal excitations, i.e., progressive deblocking, occurs at about 180 K. The blocking temperature, which is defined by the center of the peak, amounts to $T_B=250$ K.

In the FC magnetization curve, M_{CoO} amounts to 73% of the saturation magnetization M_S at the lowest temperature of 10 K (see right scale of Fig. 1). With increasing temperature, M_{CoO} decreases and reaches a local minimum of $0.52M_S$ at 180 K. With further increasing temperature a peak develops which coincides with the peak in the ZFC magnetization curve above 240 K. Deblocking of the AFM order in the CoO particles is thus the same for the ZFC and the FC case.

According to common properties of magnetic particle systems, the FC magnetization shown in Fig. 1 can be explained as follows. Deblocking of the AFM order in the particles sets in at about 180 K and peaks at $T_B=250$ K. At 180 K, the spin configuration is stable against thermal excitations and small external fields. The magnetization of about $0.5M_S$ corresponds to the remanent magnetization M_R of noninteracting single domain particles having uniaxial anisotropy with random orientation. The increased magnetization at temperatures below 180 K can be explained by interparticle interaction.[25–27] The latter continuously increases with decreasing temperature.

Further support for this interpretation is provided by temperature dependent ZFC and FC hysteresis loops. In the superparamagnetic state [Fig. 2(a)], small external fields are sufficient to reach saturation magnetization. The coercive field, i.e., one half of the loop width, is almost negligible. With decreasing temperature, the coercive field H_C and the irreversibility field H_{IRR}, i.e., the field where the hysteresis loop closes, increase. The curvature of the hysteresis loops also increases. For $T=180$ K [Fig. 2(b)], the field range of magnetization reversal is typical for particles with magnetic anisotropy of moderate strength. The remanent magnetization of $M_R=0.50M_S$ corresponds to the value of noninteracting single domain particles with random uniaxial anisotropy. With further decreasing temperature, H_C and H_{IRR} strongly increase, reaching values of $H_C=3.35$ kOe and $H_{\text{IRR}}=20-22$ kOe at $T=10$ K in the ZFC case [Fig. 2(c)].

As for the magnetization curves, interparticle interaction becomes apparent from FC measurements. For the FC hysteresis loops, the remanent magnetization M_R of the decreasing field branch continuously increases,[28] reaching a value of $0.79M_S$ at $T=10$ K [Fig. 2(d)].

The circular arrangements of arrows, included close to the experimental data in Figs. 1 and 2, schematically illustrate the effect of interparticle interaction. For simplicity, a two-dimensional picture is chosen. The net magnetization of the particles which are assumed to be single domain and the uniaxial anisotropy are shown as solid arrows and dashed lines, respectively. Both possess random orientations. At

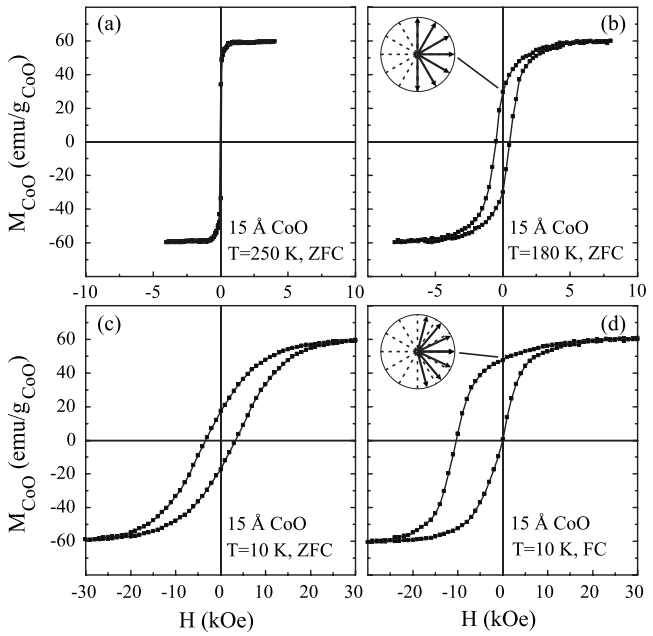

FIG. 2. ZFC and FC hysteresis loops of $[15\ \text{Å}\ \text{CoO}/60\ \text{Å}\ \text{Au}]_{20}$ at different temperatures T.

$T=180$ K [Figs. 1 and 2(b)], the magnetic moments are parallel to the local uniaxial anisotropy axes in the remanent state. All moments point in the direction of one hemisphere (i.e., all solid arrows are pointing from the left to the right), since all moments are initially pulled in the direction of the positive external field. At $T=10$ K [Figs. 1 and 2(d)], interparticle interaction leads to a rotation of the local particle magnetizations (solid arrows) closer to the direction of the initial cooling field. As a consequence, the directions of the magnetizations deviate from the local anisotropy axes (dashed lines) in the remanent state. The overall spin structure is noncollinear with characteristic tipping angles depending on the relative strength of anisotropy and interparticle interaction. For strong random uniaxial anisotropy, M_R approaches $0.5M_S$. For strong interparticle interaction, M_R approaches M_S. This behavior is related to so-called "speromagnetic" and "asperomagnetic" states in spin glasses.[18,29] It is discussed in more detail in Sec. IV.

In addition to an increase in remanent magnetization, a pronounced hysteresis loop shift occurs at lower temperatures. It amounts to $H_E=5.15$ kOe at $T=10$ K [Fig. 2(d)]. The temperature dependence of the exchange bias field H_E is summarized in Fig. 3. As a first approximation, it can be described by a linear behavior of the type $H_E \propto (1-T/T_{HE})$, with T_{HE} being the temperature at which H_E vanishes. An approximately linear falloff of the exchange bias field H_E with temperature is very common. It has been found in various kinds of material systems including particles,[5] spin glasses,[30] and bilayer films.[4,31]

Similarly, the coercivity can be approximated by a linear falloff of the type $H_C \propto (1-T/T_{HC})$. $T_{HE} \approx 150$ K is smaller than $T_{HC} \approx 200$ K because an exchange bias field only occurs if an appreciable amount of the AFM CoO spins remains fixed in the spin configuration obtained by the field-cooling process. An increase in coercivity can occur even if

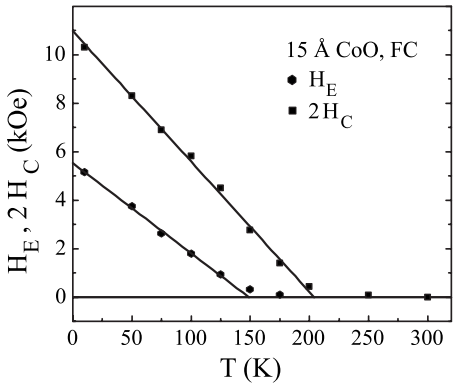

FIG. 3. Loop shift (H_E) and loop width ($2H_C$) of $[15\ \text{Å}\ \text{CoO}/60\ \text{Å}\ \text{Au}]_{20}$ as a function of temperature T for field-cooling. Solid lines have been fitted.

the AFM spins are reversed by the external field together with the net magnetic moments. H_C increases with decreasing temperature together with the magnetic anisotropy. H_E has a similar temperature dependence on the magnetic anisotropy but the additional condition of a "frozen" AFM spin configuration has to be fulfilled. In other words, in order to obtain a nonvanishing H_E, the AFM order has to be stable against thermal excitations and against the external fields which are applied during the hysteresis loop measurement.

IV. INTERACTING DEFECTS-RANDOM ANTIFERROMAGNETIC MATRIX MODEL

Based on the results obtained by the magnetization and hysteresis loop measurements, a model of exchange bias is proposed. It relies on interacting magnetic defects which are embedded in an AFM matrix with a high degree of disorder in the spatial distribution of the magnetic sublattices. This type of AFM matrix is provided by the magnetic particles having random uniaxial anisotropy. A schematic illustration of the different spin configurations obtained on the basis of this model is given in Fig. 4. The spin configuration depends on temperature, cooling procedure, and external field. Four different regimes (I–IV) are distinguished according to the critical temperatures. They correspond to the regimes I–IV given at the top of Fig. 1.

Regime I lies above the bulk Néel temperature $T_{\text{AFM},N}$ of the antiferromagnet. In this temperature regime, there exists no remanent magnetization but the net magnetization can be completely aligned by external fields of a few kOe.[28]

The net magnetization that occurs in AFM systems with reduced spatial dimensions is usually assigned to "uncompensated moments.[3]" Magnetic moments of one antiferromagnetic sublattice are called uncompensated if moments of the other antiferromagnetic sublattice, oriented into the opposite direction and therefore compensating the moment from the first sublattice, are missing. Because the net magnetization persists above the AFM ordering temperature $T_{\text{AFM},N}$, i.e., in the paramagnetic state of the bulk antiferromagnet, the term "uncompensated moments" is avoided here. This distinction is supported by recent experimental findings in other exchange bias systems using element specific

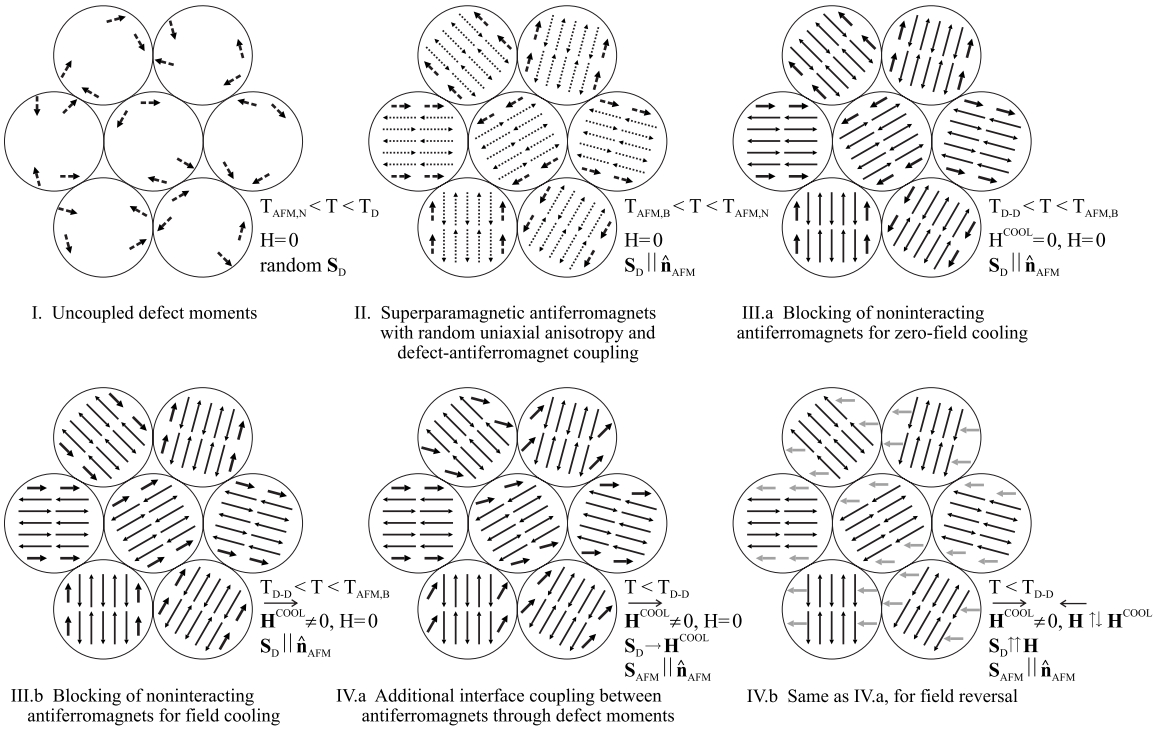

FIG. 4. Schematic illustration of the interacting defects in a random antiferromagnetic matrix model of exchange bias, shown for simplicity in a two-dimensional picture. Thermal instability of magnetic moments is indicated by dashed arrows. Positive external fields parallel H^{COOL} are pointing from left to right. For further details, see text.

synchrotron-radiation methods. In CoO/Fe bilayer films, ferromagnetic Co moments have been detected by x-ray resonant magnetic scattering at $T=300$ K which is above $T_{\mathrm{AFM},N}$ of CoO.[32] Similarly, Fe and Mn moments have been detected in the paramagnetic state of the AFM material by x-ray magnetic circular dichroism in FeMn/Co bilayer films.[33]

The net magnetization is strongly connected with the antiferromagnet and its characteristic properties, especially with respect to magnetic anisotropy and exchange interaction. On the other hand, it possesses some properties which considerably differ from antiferromagnetic behavior as outlined in detail below. A clear differentiation is therefore reasonable. The term "uncompensated moments" is avoided and the term "magnetic defect moments" is used instead. T_D is defined as the temperature at which the defect (D) moments vanish.

In Fig. 4, defect moments are shown as short bold arrows. The AFM sublattice magnetizations are shown as long thin arrows with opposite directions. Thermal instability of these moments is indicated by dashed instead of solid arrows.

In regime I ($T_{\mathrm{AFM},N}<T<T_D$), only magnetic defect moments exist. The corresponding spins $\mathbf{S}_D$ have random orientations because there is no anisotropy or interaction which is stable against thermal excitations (top left in Fig. 4). The remanent magnetization is zero.

In regime II ($T_{\mathrm{AFM},B}<T<T_{\mathrm{AFM},N}$), AFM order occurs in the particles. The spin moments $\mathbf{S}_{\mathrm{AFM}}$ of the AFM sublattices are parallel to the random directions $\hat{\mathbf{n}}_{\mathrm{AFM}}$ of the uniaxial anisotropy axes. Due to thermal instability of the AFM magnetization within each particle, $\mathbf{S}_{\mathrm{AFM}}$ and $\mathbf{S}_D$ switch between two equivalent lowest energy states which are determined by the uniaxial anisotropy axis. The overall behavior is superparamagnetic. The defect moments move together with the AFM sublattice magnetization because they are coupled to each other by an exchange interaction $J_{D\text{-AFM}}$. $J_{D\text{-AFM}}$ is assumed to be related to but not the same as the intrinsic exchange interaction of the AFM material J_{AFM} which is the origin of the antiparallel orientation of the magnetic sublattices ($J_{\mathrm{AFM}}<0$, $J_{D\text{-AFM}}<0$, $J_{\mathrm{AFM}}\neq J_{D\text{-AFM}}$). In Fig. 1, the peak centered at 250 K is most characteristic for this regime.

In regime III ($T_{D\text{-}D}<T<T_{\mathrm{AFM},B}$), the AFM and defect magnetizations are blocked along the uniaxial anisotropy axes. In Fig. 4, dashed arrows become solid arrows. As for regime II, $\mathbf{S}_D$ and $\mathbf{S}_{\mathrm{AFM}}$ are parallel to $\hat{\mathbf{n}}_{\mathrm{AFM}}$. For zero-field cooling ($H^{\mathrm{COOL}}=0$), the macroscopic net magnetization is zero because the defect spins $\mathbf{S}_D$ are parallel to $\hat{\mathbf{n}}_{\mathrm{AFM}}$ and randomly oriented in space (top right in Fig. 4). The distribution of moment directions covers a full sphere. For field-cooling ($H^{\mathrm{COOL}}\neq 0$), the defect moments are aligned by the external field during the cooling process. Field-cooling from above the AFM ordering temperature leads to freezing of the spin configuration of the antiferromagnetic matrix into a state that accommodates to the orientation of the defect moments due to the interaction $J_{D\text{-AFM}}$. Therefore, all defect spins $\mathbf{S}_D$ point in the direction of one hemisphere in the remanent state. At the bottom left in Fig. 4, all defect moments are oriented from the left to the right. The macroscopic net magnetization takes the value of $0.5M_S$ corresponding to noninteracting single domain particles with random uniaxial anisotropy. In Fig. 1, the local minimum in the FC magnetization at 180 K is most characteristic for this regime, and in Fig. 2(b), the remanent magnetization of about $0.5M_S$.

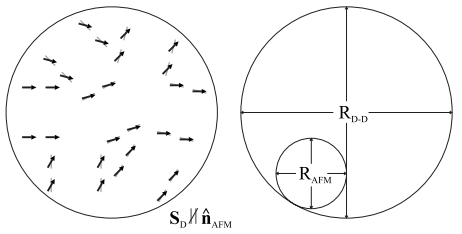

FIG. 5. Supplement to Fig. 4. Left: spatial distribution of the remanent net magnetization due to defect moments at low temperatures after field-cooling and corresponding uniaxial anisotropy axes as gray lines. Right: magnetic correlation lengths of the antiferromagnets (R_{AFM}) and of the interacting defect moments ($R_{D\text{-}D}$).

In regime IV ($T<T_{D\text{-}D}$), interparticle interaction occurs. The antiferromagnetic particles interact across the interfaces through the defect moments. The exchange interaction $J_{D\text{-}D}$ sets in at the critical temperature $T_{D\text{-}D}$ and prefers a parallel alignment of the defect moments. The defect-defect interaction competes with the coupling of the defect to the AFM order in the particles. The latter comprises the exchange interaction $J_{D\text{-AFM}}$ and, additionally, an induced uniaxial anisotropy $k_{D\text{-AFM}}$. The existence of $k_{D\text{-AFM}}$ is a consequence of the strong relationship between the defect moments and the AFM order. The defect moments are connected with the AFM order but they are also responsible for the coupling between the particles. Therefore, $J_{D\text{-AFM}}$ and $k_{D\text{-AFM}}$ are related, but not the same as J_{AFM} and k_{AFM}, which are the intrinsic exchange and anisotropy of the AFM material. If $J_{D\text{-}D}$ has a similar magnitude as $J_{D\text{-AFM}}$ and $k_{D\text{-AFM}}$, then defect moments rotate closer to the direction of the initial cooling field H^{COOL}. Assuming that J_{AFM} and k_{AFM} are large compared to $J_{D\text{-AFM}}$, the AFM sublattice magnetization remains fixed which is illustrated in IV.a and IV.b of Fig. 4. In this way, the particles form a "frozen" AFM matrix with a high degree of disorder in the spatial distribution of the magnetic sublattice. $\mathbf{S}_{\mathrm{AFM}}$ remains parallel to $\hat{\mathbf{n}}_{\mathrm{AFM}}$.

Contrary to this, $\mathbf{S}_D$ is no longer parallel to $\hat{\mathbf{n}}_{\mathrm{AFM}}$ in the remanent state (bottom center in Fig. 4). The degree of rotation is determined by the relative strength of the interparticle interaction $J_{D\text{-}D}$ and the defect-antiferromagnet coupling given by $J_{D\text{-AFM}}$ and $k_{D\text{-AFM}}$. The defect moments are collinear if $J_{D\text{-}D}$ is large compared to the other coupling contributions. Otherwise, a noncollinear spin structure results, as illustrated on the left of Fig. 5. For $k_{D\text{-AFM}}$ $(J_{D\text{-AFM}}) \gg J_{D\text{-}D}$, a magnetically disordered, spin-glass-like, state develops.

If a sufficiently large external field H is applied opposite to the cooling field H^{COOL}, the direction of the defect moments is reversed whereas the AFM matrix remains in the frozen state. In the spin configuration shown at the bottom right of Fig. 4, the reversal of the defect moments is illustrated by gray arrows.

In regime IV, two characteristic length scales exist (right in Fig. 5). One is given by the size of the particles which provides an upper limit for the antiferromagnetic correlation length R_{AFM}. This is the length of short-range structural order. The other, $R_{D\text{-}D}$, is given by the area over which the defect-defect interaction is maintained. The angles between adjacent defect moments may only slightly differ owing to the exchange while long-range magnetic order may be destroyed by the random anisotropy.[34] $R_{D\text{-}D}$ increases with increasing $J_{D\text{-}D}$ and decreasing $k_{D\text{-AFM}}$.

Most characteristic for regime IV, and particularly for the interparticle interaction $J_{D\text{-}D}$, are the increase in magnetization in the FC curve (Fig. 1) and the increased remanence in the FC hysteresis loop [Fig. 2(d)] for low temperatures. At $T=10$ K, the corresponding magnetizations amount to $0.73M_S$ and $0.79M_S$, respectively. They are considerably higher than the value of $0.5M_S$ for noninteracting single domain particles with random uniaxial anisotropy.

It should be stressed that the model and the two-dimensional spin configurations shown in Fig. 4 rely on several simplifications. In real three-dimensional systems, the arrangement of both the defect and the antiferromagnetic moments is more complicated, especially at the boundaries of and the interfaces between the particles. Additionally, more complex exchange interactions exist among the moments. Interparticle interaction is likely not exclusively ferromagnetic. Frustrated exchange and an increased magnetic disorder would be a consequence of these microscopic effects. Moreover, not all defect and antiferromagnetic sublattice moments within one particle behave in the same way.

Despite important simplifications, the assumptions made in the "interacting defects in a random antiferromagnetic matrix model" appear to be appropriate to describe the main macroscopic magnetic properties observed experimentally. The corresponding Hamiltonian is given by

$$\mathcal{H} = \mathcal{H}_D + \mathcal{H}_{D\text{-}D} + \mathcal{H}_{D\text{-AFM}} + \mathcal{H}_{\mathrm{AFM}}, \tag{1}$$

$$\mathcal{H}_D = -\mathbf{H}\sum_{i\in D}\mathbf{S}_{D,i}, \tag{2}$$

$$\mathcal{H}_{D\text{-}D} = -J_{D\text{-}D}\sum_{\langle i,j\rangle\in D}\mathbf{S}_{D,i}\mathbf{S}_{D,j}, \tag{3}$$

$$\mathcal{H}_{D\text{-AFM}} = -J_{D\text{-AFM}}\sum_{i\in D}\mathbf{S}_{D,i}\mathbf{S}_{\mathrm{AFM},i} - k_{D\text{-AFM}}\sum_{i\in D}(\mathbf{S}_{D,i}\hat{\mathbf{n}}_{\mathrm{AFM},i})^2, \tag{4}$$

$$\mathcal{H}_{\mathrm{AFM}} = -J_{\mathrm{AFM}}\sum_{\langle k,l\rangle\in \mathrm{AFM}}\mathbf{S}_{\mathrm{AFM},k}\mathbf{S}_{\mathrm{AFM},l} - k_{\mathrm{AFM}}\sum_{k\in \mathrm{AFM}}(\mathbf{S}_{\mathrm{AFM},k}\hat{\mathbf{n}}_{\mathrm{AFM},k})^2. \tag{5}$$

$\mathcal{H}_D$, $\mathcal{H}_{D\text{-}D}$, $\mathcal{H}_{D\text{-AFM}}$ describe, respectively, the interaction of the defect moments with the external field $\mathbf{H}$, the interactions among the defects, and the interaction of the defects with the antiferromagnets. $\mathcal{H}_{\mathrm{AFM}}$ contains the properties of the antiferromagnets. $J_{D\text{-}D}$, $J_{D\text{-AFM}}$, and J_{AFM} are, respectively, the exchange constants for the interactions between the defects moments, between the defect moments and the antiferromagnets, and between the antiferromagnetic moments. $J_{D\text{-}D}$ is ferromagnetic (>0), J_{AFM} antiferromagnetic (<0). $J_{D\text{-AFM}}$ is likely, but not necessarily, antiferromagnetic. $\hat{\mathbf{n}}_{\mathrm{AFM}}$ is a random easy axis direction. $k_{D\text{-AFM}}$ and k_{AFM} are the corresponding uniaxial anisotropy constants. Average values are assumed for the exchange and the anisotropy constants. The i

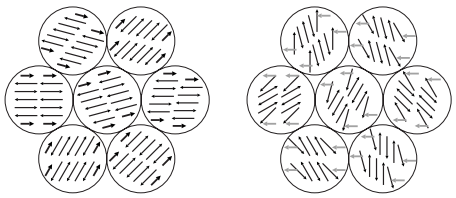

FIG. 6. Same as IV.a and IV.b in Fig. 4, for partly movable AFM sublattice magnetizations instead of an unchangeable, frozen AFM state.

and k sums are taken over all defect and all antiferromagnetic moments, respectively, $\langle i,j\rangle$ and $\langle k,l\rangle$ over the corresponding nearest neighbors. A defect spin indexed i is coupled to only one nearest antiferromagnetic spin.

Under the assumption of an unchangeable, frozen AFM matrix, the term $\mathcal{H}_{\mathrm{AFM}}$ has an important indirect effect on the magnetic behavior because the antiferromagnetic moments are fixed due to large values of J_{AFM} and k_{AFM}. As already discussed above, all spins $\mathbf{S}_D$ coupled to frozen neighboring spins $\mathbf{S}_{\mathrm{AFM}}$ point in the direction of one hemisphere defined by the direction of $\mathbf{H}^{\mathrm{COOL}}$. This is a consequence of the field-cooling procedure and can be interpreted as a directional freezing of the AFM matrix into a state that causes pinning of the defect spins. It leads to an unidirectional energy contribution for the reversal of the defects spins $\mathbf{S}_D$. In the FC hysteresis loops [Fig. 2(d)], the exchange interactions $J_{D\text{-AFM}}$ and $J_{D\text{-}D}$ are responsible for the shift H_E and thus provide the origin of the exchange bias effect. The loop width results from the anisotropy $k_{D\text{-AFM}}$ which is induced in the defect moments by to the strong coupling to the antiferromagnet. For the FC magnetization curve (Fig. 1), an increase in $J_{D\text{-}D}$ explains the increase in remanent magnetization with decreasing temperature (from $0.52M_S$ to $0.73M_S$ between 180 and 10 K). The two contributions to the term $\mathcal{H}_{\mathrm{AFM}}$ are directly involved in the magnetic behavior at higher temperatures, particularly at the blocking temperature $T_{\mathrm{AFM},B}$ and the bulk Néel temperature $T_{\mathrm{AFM},N}$.

If the AFM matrix does not remain completely frozen in an ideal spin configuration as schematically illustrated at the bottom center and bottom right of Fig. 4, the Hamiltonian in Eq. (1) has to be modified. The basic ideas of the "interacting defects in a random antiferromagnetic matrix model" are maintained but the corresponding spin structures appreciably change. Noncollinearities occur within the antiferromagnetic particles as schematically illustrated in Fig. 6. The AFM spins $\mathbf{S}_{\mathrm{AFM}}$ partly rotate with the defect spins $\mathbf{S}_D$ but the inner main part of the AFM spins remains close to the directions given by the uniaxial anisotropy k_{AFM}. Under these assumptions, the macroscopic magnetic properties, such as the shift H_E and the enhanced width H_C of the hysteresis loop, can also be explained but the relation to the microscopic properties is no longer as straightforward.

In single domain particles of larger size, a partial domain wall may develop which has a similar origin as partial domain walls in AFM/FM bilayers.[14,35,36] But for the latter, the domain wall is usually assumed to be parallel to the interface, i.e., with parallel spins within a layer plane, which has to be distinguished from spin rotation within the plane as shown in Fig. 6. However, the formation of a partial domain wall is unlikely for the present system due to the relatively small size of the CoO particles.

The present model is based on our preceding approach in Ref. 20. There are two main differences which are the defect-defect interaction across the particle interfaces and the postulation of the existence of a frozen antiferromagnetic matrix. These new assumptions are essential for a more appropriate description of the magnetic properties. In Ref. 20, random anisotropy has been concluded to be the main source of exchange bias but the underlying microscopic mechanisms have not been explained in detail. Here, a microscopic description on the basis of the Hamiltonian in Eqs. (1)–(5) is provided.

V. MONTE CARLO SIMULATIONS

Further simplifications of the model allow for the simulation of magnetic hysteresis loops by Monte Carlo (MC) methods. The defect spins $\mathbf{S}_D$ are replaced by one defect moment $\mathbf{m}_D$ for each particle and each particle interacts with its nearest neighbors. Considering only the first four terms of Eq. (1) leads to the Hamiltonian,

$$\mathcal{H} = -\mathbf{H}\sum_p \mathbf{m}_{D,p} - J'_{D\text{-}D}\sum_{\langle p,q\rangle} \mathbf{m}_{D,p}\mathbf{m}_{D,q} - J'_{D\text{-AFM}}\sum_p \mathbf{m}_{D,p}\hat{\mathbf{n}}_{\mathrm{AFM},p} - k'_{D\text{-AFM}}\sum_p (\mathbf{m}_{D,p}\hat{\mathbf{n}}_{\mathrm{AFM},p})^2. \tag{6}$$

The p sums are taken over all particles. The sum in the second term runs over nearest neighbors only.

The Hamiltonian in Eq. (6) is based on the assumption that the defect spins are embedded in an unchangeable, frozen AFM matrix which provides a high degree of spatial magnetic disorder due to random uniaxial anisotropy. The latter property is inherent in the last two terms of $\mathcal{H}$. The AFM matrix is defined by the spatial distribution of random unit vectors $\hat{\mathbf{n}}_{\mathrm{AFM}}$.

Monte Carlo simulations have been performed for a monolayer of 16×16 particles arranged in a simple two-dimensional hexagonal lattice. The number of nearest neighbors is thus $\nu=6$. The particle moments are set to one: $|\mathbf{m}_{D,p}|=1$. The standard Metropolis algorithm with local dynamics[10,25] has been used to calculate the orientation of the particle moments in metastable states responsible for hysteresis. All the details of the simulation procedure are given in Ref. 37.

ZFC and FC hysteresis loops have been calculated for different ratios of the uniaxial anisotropy and the interparticle interaction. For both ZFC and FC loops, the remanent magnetization increases with decreasing $k'_{D\text{-AFM}}/J'_{D\text{-}D}$ due to the ferromagnetic exchange interaction $J'_{D\text{-}D}$. The coercivity H_C and the irreversibility field H_{IRR} decrease with decreasing $k'_{D\text{-AFM}}/J'_{D\text{-}D}$ due to the relative decrease in magnetic anisotropy. H_C is approximately proportional to, and of the order of magnitude of, $k'_{D\text{-AFM}}$. For larger $k'_{D\text{-AFM}}/J'_{D\text{-}D}$, H_{IRR} reaches $k'_{D\text{-AFM}}+J'_{D\text{-AFM}}$ which corresponds to the maximum energy barrier due to the matrix-induced anisotropy and exchange.

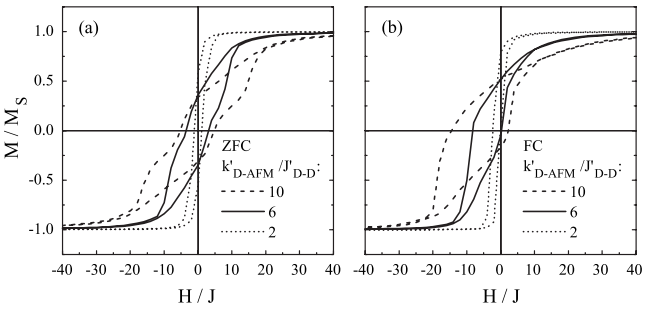

FIG. 7. Calculated ZFC (a) and FC (b) hysteresis loops of the model explained in the text for different ratios of the random uniaxial anisotropy $k'_{D\text{-AFM}}$ ($J'_{D\text{-AFM}}=k'_{D\text{-AFM}}$) and the interparticle exchange interaction $J'_{D\text{-}D}$.

For field-cooling, the directions of the interaction $J'_{D\text{-AFM}}$ are chosen under the condition that all defect moments point in the direction of one hemisphere in the remanent state. $\hat{\mathbf{n}}_{\text{AFM}}$ is thus randomly oriented in space but always points in directions distributed around the direction of $\mathbf{H}^{\text{COOL}}$. As already discussed in Sec. IV, this can be interpreted as a directional freezing of the AFM matrix into a state that causes pinning of the defect moments. The directional freezing is responsible for the symmetry breaking in the magnetization reversal process. It leads to an unidirectional anisotropy and therefore to the loop shift H_E. Mirror symmetry breaking is not inherent in the Hamiltonian in Eq. (6) itself.

A good correspondence between the experimental behavior at $T=10$ K [Figs. 2(c) and 2(d)] and the MC simulation is obtained for $k'_{D\text{-AFM}}=J'_{D\text{-AFM}}=6J'_{D\text{-}D}$ [solid lines in Figs. 7(a) and 7(b)].[37] In this case, the magnitude of the total interparticle exchange energy $\nu J'_{D\text{-}D}=6J'_{D\text{-}D}$ is of the same magnitude as the anisotropy energy $k'_{D\text{-AFM}}$ and smaller than the total defect-antiferromagnet coupling energy $k'_{D\text{-AFM}}+J'_{D\text{-AFM}}$.

VI. MAGNETIC PROPERTIES OF COBALT OXIDE/FERROMAGNET BILAYERS

The "interacting defects in a random antiferromagnetic matrix model" provides an approach to the problem of exchange bias not only for antiferromagnetic particle systems but also for antiferromagnetic/ferromagnetic bilayers. CoO/ferromagnet bilayers, for example, have many properties in common with the granular CoO/Au multilayers of Sec. III.

In Figs. 8(a)–8(c), FC hysteresis loops at $T=10$ K are shown for CoO/Fe, CoO/Co, and CoO/Ni bilayers. They are characterized by loop shifts H_E and enhanced half-loop widths H_C of similar magnitude. The exchange bias energy $\Delta E=H_E M_{\text{FM}} t_{\text{FM}}$ (Ref. 3) which is independent of FM magnetization M_{FM} and FM layer thickness t_{FM} amounts to 0.93, 1.03, and 0.80 erg/cm^2 for CoO/Fe, CoO/Co, and CoO/Ni, respectively.

Independent of FM material, the temperature dependence of the exchange bias field H_E shows an approximately linear falloff [Figs. 8(d)–8(f)]. Fitting a linear behavior of the type $H_E \propto (1-T/T_{HE})$ results in a common value of T_{HE} of about 170 K.

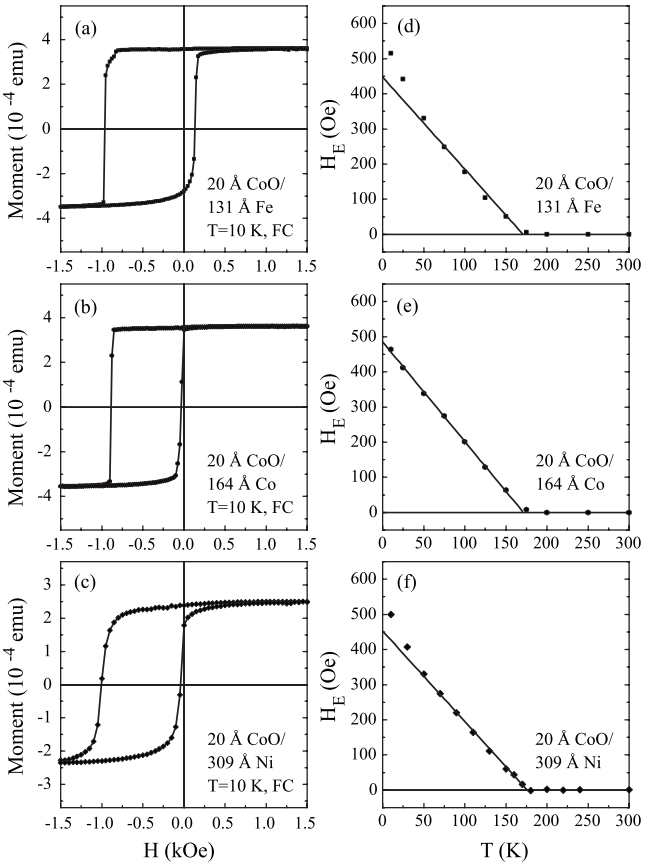

FIG. 8. FC hysteresis loops at $T=10$ K (left) and loop shifts H_E as function of temperature T (right) for 20 Å CoO/x Å FM bilayers with FM=Fe, Co, Ni. Solid lines in (d)–(f) have been fitted.

The similar temperature dependence of the exchange bias field H_E, the similar hysteresis loop shape, and the similar exchange coupling energy ΔE for different ferromagnetic materials lead to the conclusion that the magnetization reversal behavior of the CoO/FM bilayers is dominated by properties of the CoO.

Moreover, the CoO/FM bilayers have important magnetic properties in common with the CoO particle layers. Both magnetic systems show an approximately linear falloff of the type $H_E \propto (1-T/T_{HE})$ for the exchange bias field with a similar value of T_{HE}. Similarities also exist in the magnetization reversal behavior, i.e., in the shape and shift of the hysteresis loop. The dominance of the antiferromagnet on the magnetization reversal of the ferromagnet is particularly pronounced in the second hysteresis loop as shown in Fig. 9(a) for a CoO/Fe bilayer.

According to the "interacting defects in a random antiferromagnetic matrix model," magnetic hysteresis behavior in granular CoO/ferromagnetic bilayers follows from coupling of the ferromagnet to the net particle magnetization in the disordered antiferromagnetic CoO. The Hamiltonian in Eq. (1) has thus to be extended by the properties of the ferromagnetic layer,

$$\mathcal{H}=\mathcal{H}_D+\mathcal{H}_{D\text{-}D}+\mathcal{H}_{D\text{-AFM}}+\mathcal{H}_{\text{AFM}}+\mathcal{H}_{D\text{-FM}}+\mathcal{H}_{\text{FM}}, \quad (7)$$

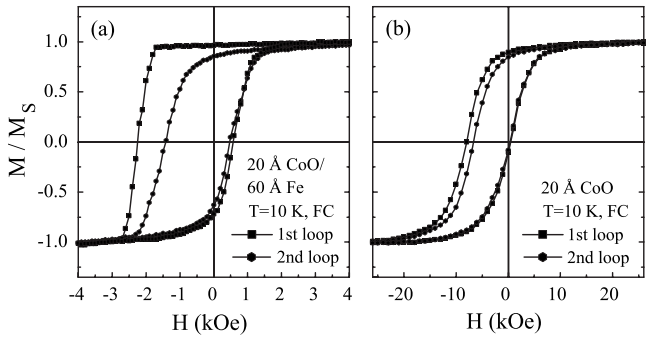

FIG. 9. FC hysteresis loops at $T=10$ K for a 20 Å CoO/60 Å Fe bilayer (left) and $[20\ \text{Å CoO}/60\ \text{Å Au}]_{20}$ (right). First and second loops, i.e., training effects (Ref. 38) are shown.

$$\mathcal{H}_{D\text{-FM}} + \mathcal{H}_{\text{FM}} = -\sum_{i\in D} J_{D\text{-FM},i}\mathbf{S}_{D,i}\mathbf{S}_{\text{FM},i} - J_{\text{FM}}\sum_{\langle m,n\rangle\in\text{FM}} \mathbf{S}_{\text{FM},m}\mathbf{S}_{\text{FM},n} - \mathbf{H}\sum_{m\in\text{FM}} \mathbf{S}_{\text{FM},m}. \tag{8}$$

$\mathcal{H}_{D\text{-FM}}$ describes the coupling of the nearest ferromagnetic spins $\mathbf{S}_{\text{FM}}$ to the defect spins $\mathbf{S}_D$ of the antiferromagnet by an exchange interaction $J_{D\text{-FM}}$. It is assumed that $J_{D\text{-FM}}$ is mainly ferromagnetic similar to the interparticle interaction $J_{D\text{-}D}$. No average value is assigned because $J_{D\text{-FM}}$ strongly depends on the distance between $\mathbf{S}_{\text{FM}}$ and $\mathbf{S}_D$. $\mathcal{H}_{\text{FM}}$ contains the exchange interaction J_{FM} among the ferromagnetic spins and the interaction with the external field $\mathbf{H}$.

For the first loop in Fig. 9(a) and the loops in Figs. 8(a)–8(c), the reversal of the ferromagnet opposite to the initial cooling field $\mathbf{H}^{\text{COOL}}$ is dominated by a strong coupling J_{FM} between the ferromagnetic spins. All $\mathbf{S}_{\text{FM}}$ remain collinear. For the second loop, on the contrary, the reversal is dominated by the coupling $J_{D\text{-FM}}$ to the CoO. The almost rectangular shape of the hysteresis loop changes to a strongly curved shape which is typical for training effects in CoO/ferromagnet bilayers.[38] The similarities of the hysteresis loops for CoO/ferromagnet bilayers and CoO particle layers [Figs. 9(a) and 9(b)] indicate that the noncollinearities in the spin structure of the CoO also determine the magnetic behavior of the CoO/ferromagnet bilayers. The reduced magnetic correlation length within the antiferromagnet plays a decisive role in this context.

VII. SUMMARY

Temperature dependent magnetization curves and magnetic hysteresis loops of CoO particle layers show characteristic features which can be attributed to different critical temperatures and different exchange interactions involving interparticle interaction by defect moments. CoO particle layers have important magnetic properties in common with CoO/ferromagnet bilayers. For both magnetic systems, the temperature dependence of the exchange bias field shows an approximately linear falloff with a common critical temperature. Strong correlations also exist in the magnetization reversal behavior.

On the basis of the experimental results, an approach to the problem of exchange bias is suggested. It relies on interacting magnetic defects which are embedded in an antiferromagnetic matrix with a high degree of disorder in the spatial distribution of the magnetic anisotropy. The matrix is provided by the antiferromagnetic particles, the disorder by their randomness in anisotropy.

Under the assumption of an unchangeable, frozen antiferromagnetic matrix, the exchange interaction $J_{D\text{-AFM}}$ between the defects and the antiferromagnet and the defect-defect interaction $J_{D\text{-}D}$ are responsible for the hysteresis loop shift H_E. They thus provide the origin of the exchange bias effect. The loop width results from the anisotropy $k_{D\text{-AFM}}$ which is induced in the defect moments by to the strong coupling to the antiferromagnet. For the field-cooled magnetization, an increase in interparticle interaction $J_{D\text{-}D}$ explains the increase in remanence with decreasing temperature. In the remanent state, the overall spin structure of the defects is noncollinear with characteristic tipping angles depending on the anisotropy-to-exchange ratio $k_{D\text{-AFM}}/J_{D\text{-}D}$.

The "interacting defects in a random antiferromagnetic matrix model" not only applies to layered systems containing antiferromagnetic particles but also to cluster and polycrystalline materials. The model is an approach to the microscopic understanding of exchange bias and has important implications for future experimental and theoretical work.

[1] W. H. Meiklejohn and C. P. Bean, Phys. Rev. **102**, 1413 (1956).
[2] W. H. Meiklejohn, J. Appl. Phys. **33**, 1328 (1962).
[3] J. Nogués and I. K. Schuller, J. Magn. Magn. Mater. **192**, 203 (1999).
[4] A. E. Berkowitz and K. Takano, J. Magn. Magn. Mater. **200**, 552 (1999).
[5] B. Martínez, X. Obradors, Ll. Balcells, A. Rouanet, and C. Monty, Phys. Rev. Lett. **80**, 181 (1998).
[6] V. Skumryev, S. Stoyanov, Y. Zhang, G. Hadjipanayis, D. Givord, and J. Nogués, Nature (London) **423**, 850 (2003).
[7] J. S. Kouvel, J. Phys. Chem. Solids **24**, 795 (1963).
[8] S. G. E. te Velthuis, G. P. Felcher, J. S. Jiang, A. Inomata, C. S. Nelson, A. Berger, and S. D. Bader, Appl. Phys. Lett. **75**, 4174 (1999).
[9] M. Hanson, C. Johansson, and S. Mørup, J. Phys.: Condens. Matter **7**, 9263 (1995).
[10] D. A. Dimitrov and G. M. Wysin, Phys. Rev. B **54**, 9237 (1996).
[11] A. P. Malozemoff, Phys. Rev. B **35**, 3679 (1987).
[12] R. L. Stamps, J. Phys. D **33**, R247 (2000).
[13] M. Kiwi, J. Magn. Magn. Mater. **234**, 584 (2001).
[14] F. Radu and H. Zabel, in *Magnetic Heterostructures*, edited by H. Zabel and S. D. Bader (Springer, Berlin, 2008), Vol. 227, p. 97.
[15] K. Takano, R. H. Kodama, A. E. Berkowitz, W. Cao, and G.

Thomas, Phys. Rev. Lett. **79**, 1130 (1997).
[16] J. Nogués, J. Sort, V. Langlais, V. Skumryev, S. Suriñach, J. S. Muñoz, and M. D. Baró, Phys. Rep. **422**, 65 (2005).
[17] R. H. Kodama and A. E. Berkowitz, Phys. Rev. B **59**, 6321 (1999).
[18] K. Moorjani and J. M. D. Coey, *Magnetic Glasses* (Elsevier, Amsterdam, 1984).
[19] U. Nowak, K. D. Usadel, J. Keller, P. Miltényi, B. Beschoten, and G. Güntherodt, Phys. Rev. B **66**, 014430 (2002).
[20] M. Gruyters, Europhys. Lett. **77**, 57006 (2007).
[21] D. Fiorani, L. Del Bianco, A. M. Testa, and K. N. Trohidou, Phys. Rev. B **73**, 092403 (2006).
[22] P. Dumas, Y. J. Chabal, R. Gunther, A. Taleb-Ibrahimi, and Y. Petroff, Prog. Surf. Sci. **48**, 313 (1995).
[23] M. Gruyters and D. Riegel, Phys. Rev. B **63**, 052401 (2000).
[24] M. Gruyters and D. Riegel, J. Appl. Phys. **88**, 6610 (2000); M. Gruyters, J. Magn. Magn. Mater. **248**, 248 (2002).
[25] J. García-Otero, M. Porto, J. Rivas, and A. Bunde, J. Appl. Phys. **85**, 2287 (1999).
[26] V. Russier, J. Appl. Phys. **89**, 1287 (2001).
[27] C. Frandsen, C. R. H. Bahl, B. Lebech, K. Lefmann, L. Theil Kuhn, L. Keller, N. H. Andersen, M. v. Zimmermann, E. Johnson, S. N. Klausen, and S. Mørup, Phys. Rev. B **72**, 214406 (2005).
[28] M. Gruyters, Phys. Rev. Lett. **95**, 077204 (2005).
[29] R. Skomski, J. Magn. Magn. Mater. **157-158**, 713 (1996).
[30] S. Schultz, E. M. Gullikson, D. R. Fredkin, and M. Tovar, Phys. Rev. Lett. **45**, 1508 (1980).
[31] A. P. Malozemoff, J. Appl. Phys. **63**, 3874 (1988).
[32] F. Radu, A. Nefedov, J. Grabis, G. Nowak, A. Bergmann, and H. Zabel, J. Magn. Magn. Mater. **300**, 206 (2006).
[33] F. Offi, W. Kuch, L. I. Chelaru, K. Fukumoto, M. Kotsugi, and J. Kirschner, Phys. Rev. B **67**, 094419 (2003).
[34] E. M. Chudnovsky, J. Appl. Phys. **64**, 5770 (1988).
[35] D. Mauri, H. C. Siegmann, P. S. Bagus, and E. Kay, J. Appl. Phys. **62**, 3047 (1987).
[36] A. Scholl, M. Liberati, E. Arenholz, H. Ohldag, and J. Stöhr, Phys. Rev. Lett. **92**, 247201 (2004).
[37] M. Gruyters, J. Magn. Magn. Mater. **320**, 407 (2008).
[38] A. Hoffmann, Phys. Rev. Lett. **93**, 097203 (2004).